

# Drones Guiding Drones: Cooperative Navigation of a Less-Equipped Micro Aerial Vehicle in Cluttered Environments

Václav Pritzl\*, Matouš Vrba\*, Yurii Stasinchuk\*, Vít Krátký\*, Jiří Horyna\*, Petr Štěpán\*, and Martin Saska\*

**Abstract**—Reliable deployment of Unmanned Aerial Vehicles (UAVs) in cluttered unknown environments requires accurate sensors for obstacle avoidance. Such a requirement limits the usage of cheap and micro-scale vehicles with constrained payload capacity if industrial-grade reliability and precision are required. This paper investigates the possibility of offloading the necessity to carry heavy and expensive obstacle sensors to another member of the UAV team while preserving the desired obstacle avoidance capability. A novel cooperative guidance framework offloading the obstacle sensing requirements from a minimalist secondary UAV to a superior primary UAV is proposed. The primary UAV constructs a dense occupancy map of the environment and plans collision-free paths for both UAVs to ensure reaching the desired secondary UAV’s goal. The primary UAV guides the secondary UAV to follow the planned path while tracking the UAV using Light Detection and Ranging (LiDAR)-based relative localization. The proposed approach was verified in real-world experiments with a heterogeneous team of a 3D LiDAR-equipped primary UAV and a camera-equipped secondary UAV moving autonomously through unknown cluttered Global Navigation Satellite System (GNSS)-denied environments with the proposed framework running completely on board the UAVs.

## MULTIMEDIA ATTACHMENT

<https://mrs.felk.cvut.cz/icra2024guiding>

## I. INTRODUCTION

The ability to accurately perceive the surrounding obstacles is crucial for aerial robots operating in cluttered environments. However, such capabilities may require the presence of heavy and expensive sensors onboard the size, weight, and power-constrained Unmanned Aerial Vehicles (UAVs). Minimizing such hardware requirements is critical when the UAVs need to be as small as possible or if a low aggregate cost of the multi-UAV team is required.

In many applications, having micro UAVs with only application-specific payload is desirable. In cooperative sensing tasks, the aim is to distribute UAVs with specific sensors to target positions to detect the sought phenomenon, such as a gas source [1]. When operating in a confined indoor environment, small UAVs with communication modules may be used to build a mesh communication network, similarly as in the breadcrumb-deploying communication solutions of the DARPA SubT challenge [2]. In Global Navigation

This work was supported by CTU grant no SGS23/177/OHK3/3T/13 and by the Czech Science Foundation (GAČR) under research project No. 23-07517S.

\*The authors are with the Multi-robot Systems Group, Department of Cybernetics, Faculty of Electrical Engineering, Czech Technical University in Prague, Czech Republic {vaclav.pritzl, matous.vrba, yuriy.stasinchuk, vit.kratky, jiri.horyna, petr.stepan, martin.saska}@fel.cvut.cz

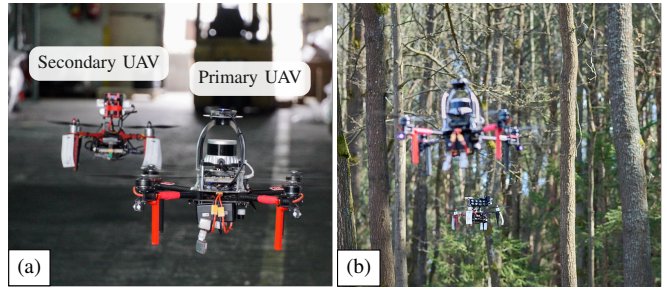


Fig. 1: The LiDAR-equipped primary UAV guides the secondary camera-equipped UAV through (a) narrow passages in an industrial complex, (b) a cluttered forest environment.

Satellite System (GNSS)-denied conditions, UAVs carrying localization anchors can be distributed to specific positions in the environment to provide an external localization system for the other robots [3]. In sensory degraded environments, the minimalist UAVs can serve as landmarks for improving the localization performance of the rest of the robot team [4]. All these tasks benefit from the ability to guide cheap miniature UAVs with only application-specific hardware to target positions or to places untraversable by the larger UAVs, either guiding them all the way or through areas too challenging for their own onboard sensors.

In this paper, we focus on offloading the obstacle sensing capability from the less-capable UAVs to a more-capable guiding UAV with superior sensors and processing power. Specifically, we deal with the case of a 3D Light Detection and Ranging (LiDAR)-equipped primary UAV guiding a smaller camera-equipped secondary UAV (see Fig. 1). LiDAR sensors exhibit significant precision and robustness to various environmental conditions but are generally heavy and expensive. Using LiDAR-based and visual-based navigation in a single UAV team combines the benefits of both approaches while mitigating their drawbacks.

### A. Problem statement

We tackle the problem of cooperative flight of two diverse UAVs in an unknown GNSS-denied cluttered environment. The primary UAV (pUAV) carries a 3D LiDAR sensor. The secondary UAV (sUAV) carries a visual camera for local self-localization only and has insufficient obstacle-sensing capabilities for the desired application. Both UAVs are equipped with an onboard computer, an Inertial Measurement Unit (IMU), an embedded attitude controller, and a wireless communication module. We assume that the 3D LiDAR provides sufficient data for precise localization with low long-term drift w.r.t. the world reference frame, while the visual

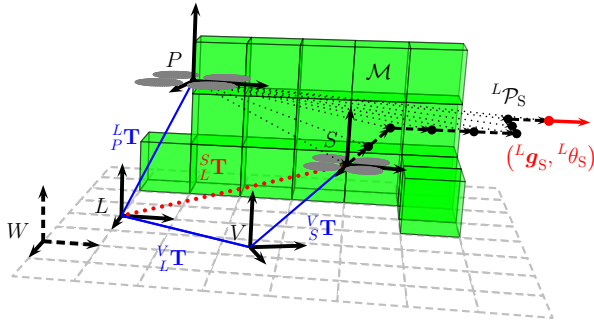


Fig. 2: The pUAV with body frame  $P$  is localized in its local frame  $L$ , builds dense occupancy map  $\mathcal{M}$ , and plans collision-free paths for both UAVs. The sUAV with body frame  $S$  is localized in its local frame  $V$ .  $W$  denotes the fixed world reference frame. All the reference frames are gravity-aligned. The pUAV periodically guides the sUAV to follow the planned path  ${}^L\mathcal{P}_S$ . Line of sight between the pUAV position and sUAV waypoints is depicted by black dotted lines.

camera data is sufficient for short-term localization, i.e., for stabilization of the UAV but may exhibit significantly larger drift than the LiDAR-based localization. Thus, relying on the LiDAR sensor for self-localization of the pUAV and relative localization between the UAVs enables precise localization for the entire UAV team. The UAVs are capable of mutual communication with the pUAV transmitting planned paths to the sUAV and the sUAV transmitting its local odometry data to the pUAV. All software runs entirely on board the UAVs with no external computational resources. Both UAVs use only their onboard sensors for localization, and no external localization system is available.

We denote vectors as bold lowercase letters, matrices as bold upright uppercase letters, and frames of reference as uppercase italic letters. Let  ${}^A\mathbf{T} \in SE(3)$  be the transformation matrix describing the transformation from frame  $A$  to frame  $B$ . Let  ${}^A\mathbf{x}$  be a 3D position vector in frame  $A$ . We denote sets and sequences by uppercase calligraphic letters. Let  ${}^A\mathcal{P}_B$  be a sequence of UAV reference poses  $({}^A\mathbf{x}_i, {}^A\theta_i)$ , consisting of position  ${}^A\mathbf{x}_i \in \mathbb{R}^3$  and heading  ${}^A\theta_i \in [-\pi, \pi]$ , for UAV  $B$  in reference frame  $A$ , thus forming a path with a specific heading assigned to each position.

The addressed problem, depicted in Fig. 2, is to guide the sUAV to a goal pose  $({}^L\mathbf{g}_S, {}^L\theta_S)$ , consisting of position  ${}^L\mathbf{g}_S \in \mathbb{R}^3$  and heading  ${}^L\theta_S \in [-\pi, \pi]$ . Specifically, the task is to plan a collision-free path  ${}^L\mathcal{P}_S$  based on the 3D occupancy map  $\mathcal{M}$  built by the pUAV and guide the sUAV along the planned path  ${}^L\mathcal{P}_S$ . Also, plan a path  ${}^L\mathcal{P}_P$  for the pUAV to ensure tracking of the sUAV throughout the environment.

### B. Related work

Utilizing heterogeneous multi-robot teams consisting of more-capable robots guiding less-capable robots has been proposed for use with Unmanned Ground Vehicles (UGVs) in the past [5]–[8]. Related works in the area of UGV-UAV cooperation have focused on the cooperation of a UGV

and a UAV acting as an “eye in the sky”, observing the UGV along with its surroundings from above [9]. From its high viewpoint, the UAV can map the surroundings of the UGV and plan a collision-free path for the UGV to follow, as proposed in [10]–[13]. In some approaches, the path planning was performed directly on the image data without map construction, with calculations being done either on the UAV [14] or in the cloud [15]. In [16], the authors proposed to solve the path planning as a Partially Observable Markov Decision Process (POMDP) without global map construction and evaluated their approach in simulations. In [17], the UAV sent only target positions to the UGV, which performed motion planning on its own sensory data. In [18], a terrain map was constructed on a ground station using a learning-based approach and sent to the UGV, which used it for path planning. In [19], the UAV shared its voxel map of the environment with a UGV, which converted the voxel map to an elevation map and utilized it for path planning. In [20], a trajectory optimization approach for a UGV guiding a UAV while maintaining visibility was proposed, motivated by scanning warehouse racks for inventory management.

To the best of our knowledge, a cooperative navigation approach offloading motion planning in a cluttered environment to another UAV has not yet been deployed in a UAV-only team despite its potential to enable more advanced distribution of the required sensors and individual capabilities among the heterogeneous UAV team. Deploying such an approach on board the UAVs is challenging due to the inherent limitations by their size, weight, and power. The UAVs moving in cluttered spaces need to plan their motion in 3D space with low processing times to utilize the limited battery life as efficiently as possible while simultaneously running their localization and control algorithms uninterruptedly at a high rate to preserve flight stability.

The approach proposed in this paper builds upon our previous work on the use of LiDAR-based detections [21] and fusion of LiDAR-based detections with Visual-Inertial Odometry (VIO) [22] for guiding a cooperating UAV. The LiDAR-based approach provides precise relative localization between the UAVs, enabling reliable guidance in the cluttered spaces. None of the above-mentioned works on UAV-UGV cooperation utilize LiDAR-based relative localization of the UAV, relying instead on visual, GNSS, or Ultra-wideband (UWB)-based methods.

The contribution of this paper can be summarized as a novel framework for the flight of a heterogeneous UAV team, effectively offloading occupancy mapping and path planning requirements to a more-capable UAV while preserving the obstacle avoidance capabilities of the less-capable UAV. The approach has been extensively verified in multiple real-world experiments in cluttered GNSS-denied environments with all algorithms running entirely on board the UAVs with no external computational resources utilized.

## II. MULTI-UAV PLANNING AND GUIDANCE

A high-level diagram of the proposed multi-UAV framework is shown in Fig. 3. The pUAV is localized using a

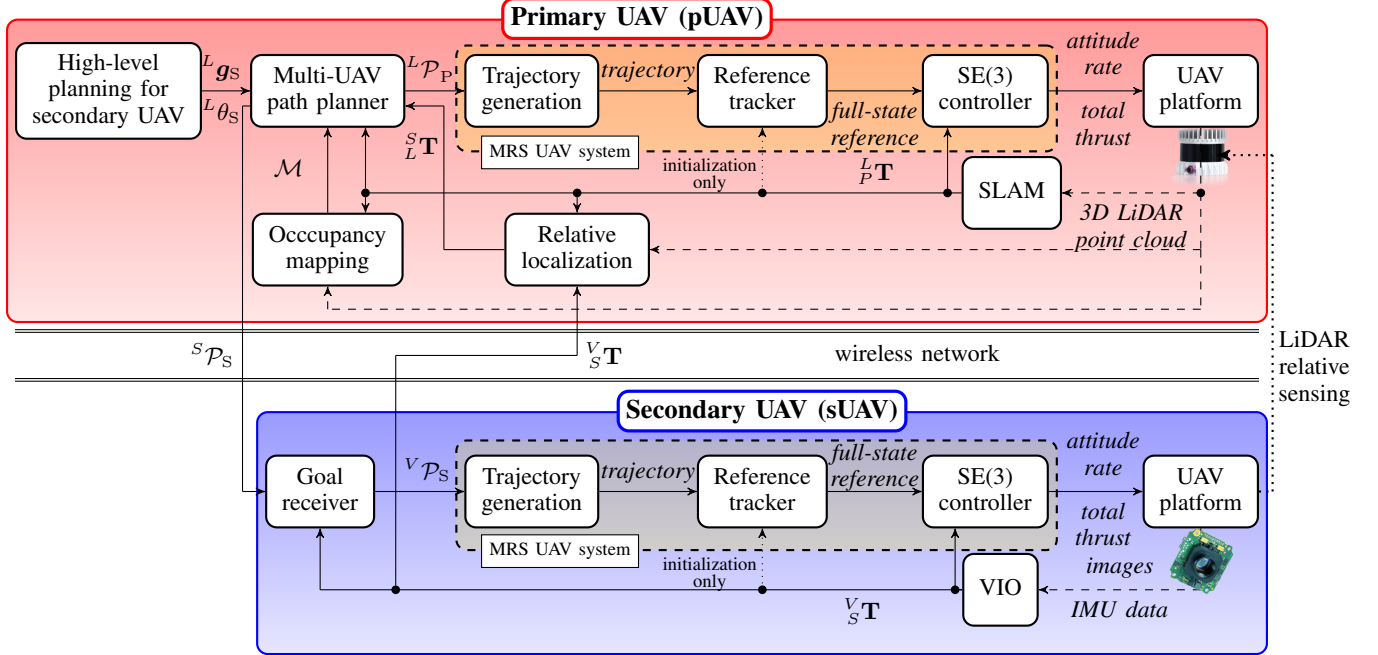


Fig. 3: The pUAV maps the surrounding environment using 3D LiDAR data, performs relative localization of the sUAV using a combination of LiDAR detections and received VIO data, and guides the sUAV to desired poses. The position control pipeline in the frame of each respective self-localization method is provided by the MRS UAV System [23].

3D LiDAR-based Simultaneous Localization and Mapping (SLAM) and performs dense occupancy mapping using the Octomap [24] approach, producing an occupancy map  $\mathcal{M}$  of the environment. To decrease the processing requirements, the map  $\mathcal{M}$  represents a limited region of the environment, centered at the current pUAV position. The sUAV uses VIO for self-localization.

Position control in the frames of the respective self-localization methods is provided by the MRS UAV System<sup>1</sup> [23]. The system times of the UAVs are synchronized over the wireless network using the Network Time Protocol (NTP). The *Multi-UAV path planner* module receives high-level sUAV goals  $(^L g_S, ^L \theta_S)$  and constructs collision-free paths for both the sUAV and the pUAV itself. The sUAV path is periodically transformed to the sUAV body frame  $S$  using the relative localization data and transmitted to the sUAV over the wireless network. During the guiding process, the pUAV-sUAV pair essentially forms a closed loop controlling the sUAV pose in the local reference frame  $L$ .

#### A. Relative localization

Accurate relative localization between the UAVs is crucial for reliable performance of the guiding approach, and uncertainty in the relative localization represents one of the main sources of guiding errors. The relative localization approach needs to accurately provide the transformation  ${}^S T$  required for transforming the reference path from the local frame  $L$  to the sUAV body frame  $S$ . In the experimental evaluation of the proposed approach, relative localization based on the

fusion of LiDAR detections [25] with VIO data received over the wireless network [22] was employed. The LiDAR detections provide precise 3D positions of the sUAV, and the fusion with VIO data provides orientation of the sUAV and keeps track of the sUAV when the detections are lost. In contrast to the approach described in [22], the sUAV was equipped with reflective markers on its legs (see Fig. 1) to aid the LiDAR-based detection approach. As the employed 3D LiDAR sensor can calculate the reflectivity of each measured data point, a thresholding-based filter was applied to filter out possible false detections and thus increase the reliability of UAV detections in cluttered environments.

#### B. Multi-UAV path planner

The *Multi-UAV path planner* module consists of a Finite-State Machine (FSM) transferring between the *IDLE*, *PLANNING*, *PRIMARY MOVING*, *SECONDARY MOVING*, *GOAL REACHED*, and *FAILURE* states. When the module receives a new goal  $(^L g_S, ^L \theta_S)$  for the sUAV, the FSM transfers to the *PLANNING* state and constructs collision-free paths  ${}^L \mathcal{P}_P, {}^L \mathcal{P}_S$  for both UAVs. In the *PRIMARY MOVING* state, the pUAV moves along its path to a viewpoint  ${}^L g_P$ , where it can observe and guide the sUAV. After reaching such a viewpoint, the FSM transfers to the *SECONDARY MOVING* state. In the *SECONDARY MOVING* state, the pUAV guides the sUAV to follow the planned collision-free path  ${}^L \mathcal{P}_S$ . When the goal is reached, the FSM transfers to the *GOAL REACHED* state.

The path planning process proceeds according to Alg. 1. The planner takes the current occupancy map  $\mathcal{M}$  and inserts an occupied region at the current position  ${}^L x_P$  of the pUAV

<sup>1</sup>[https://github.com/ctu-mrs/mrs\\_uav\\_system](https://github.com/ctu-mrs/mrs_uav_system)

---

**Algorithm 1** Multi-UAV path planning (state = *PLANNING*)

---

**Input:** Map  $\mathcal{M}$ , pUAV pose  $({}^L\mathbf{x}_P, {}^L\phi_P)$ , sUAV pose  $({}^L\mathbf{x}_S, {}^L\phi_S)$ , sUAV goal pose  $({}^L\mathbf{g}_S, {}^L\theta_S)$   
**Output:** Paths  ${}^L\mathcal{P}_P, {}^L\mathcal{P}_S$  sent to the UAVs' control pipelines  
**Parameters:** pUAV obstacle width  $w_P$  and height  $h_P$ , sUAV obstacle width  $w_S$  and height  $h_S$ , pUAV minimum obstacle distance  $d_P$ , sUAV minimum obstacle distance  $d_S$

- 1: **if**  $\|{}^L\mathbf{x}_S - {}^L\mathbf{g}_S\|_2 < \mathcal{M}.resolution$  **then**
- 2:   CHANGE\_STATE(*GOAL REACHED*)
- 3:   **return**
- 4:  $\mathcal{M}_S \leftarrow \text{COPY\_MAP\_AND\_ADD\_OBSTACLE}(\mathcal{M}, {}^L\mathbf{x}_P, w_P, h_P)$
- 5:  ${}^L\mathcal{P}_S \leftarrow \text{FIND\_PATH}(\mathcal{M}_S, {}^L\mathbf{x}_S, {}^L\phi_S, {}^L\mathbf{g}_S, {}^L\theta_S, d_S)$    ▷ Using A\* planner
- 6: **if**  ${}^L\mathcal{P}_S = \emptyset$  **then**
- 7:   CHANGE\_STATE(*FAILURE*)
- 8:   **return**
- 9:  ${}^L\mathbf{g}_P \leftarrow \text{GUIDING\_VIEWPOINT\_SELECTION}(\mathcal{M}, {}^L\mathcal{P}_S, {}^L\mathbf{x}_P)$
- 10: **if**  ${}^L\mathbf{g}_P = \emptyset$  **then**
- 11:   CHANGE\_STATE(*FAILURE*)
- 12:   **return**
- 13: **if**  $\|{}^L\mathbf{x}_P - {}^L\mathbf{g}_P\|_2 < \mathcal{M}.resolution$  **then**
- 14:   CHANGE\_STATE(*SECONDARY MOVING*,  ${}^L\mathcal{P}_S$ )
- 15:   **return**
- 16:  $\mathcal{M}_P \leftarrow \text{COPY\_MAP\_AND\_ADD\_OBSTACLE}(\mathcal{M}, {}^L\mathbf{x}_S, w_S, h_S)$
- 17:  ${}^L\mathcal{P}_P \leftarrow \text{FIND\_PATH}(\mathcal{M}_P, {}^L\mathbf{x}_P, {}^L\phi_P, {}^L\mathbf{g}_P, {}^L\theta_P, d_P)$    ▷ Using A\* planner
- 18: **if**  ${}^L\mathcal{P}_P = \emptyset$  **then**
- 19:   CHANGE\_STATE(*FAILURE*)
- 20:   **return**
- 21: CHANGE\_STATE(*PRIMARY MOVING*,  ${}^L\mathcal{P}_P$ )
- 22: **return**

---

with safety margin above and below to avoid the downwash effect. A collision-free path  ${}^L\mathcal{P}_S$  for the sUAV is planned using an A\* planner. In our framework, we have utilized the A\* planning algorithm with iterative path post-processing designed for the DARPA SubT challenge, described in [2], [26]. Based on the resulting path, a goal viewpoint  ${}^L\mathbf{g}_P$  for the pUAV is selected, such that the pUAV can observe as large portion of the sUAV path  ${}^L\mathcal{P}_S$  as possible (see sec. II-B.1 for details). Occupied space at the position  ${}^L\mathbf{x}_S$  of the sUAV is inserted to the map and the A\* planner constructs a collision-free path  ${}^L\mathcal{P}_P$  for the pUAV.

1) *Guiding viewpoint selection:* To maximize line-of-sight (LOS) visibility throughout the guiding process, a viewpoint  ${}^L\mathbf{g}_P$  for the pUAV is computed (see Alg. 2 and Fig. 4), such that it fulfills the following conditions:

- 1) The pUAV has LOS visibility of as many sUAV waypoints from the path beginning as possible. The areas with LOS visibility of the specific sUAV waypoints are represented as a set of non-convex polygons  $\mathcal{V}_{\text{all}}$ .
- 2) The closest obstacle distance is larger than a threshold  $d_P$ . This creates a safe region, represented as a multi-polygon (collection of non-convex polygons with holes and non-intersecting boundaries)  $\mathcal{S}$ .
- 3) The distance to the sUAV path  ${}^L\mathcal{P}_S$  should be larger than a desired safety threshold  $d_{\text{buffer}}$ . The safety buffer around the sUAV path is represented as a non-convex polygon  $\mathcal{B}$ .

Alg. 2 constructs 2D polygons representing the visibility

---

**Algorithm 2** Guiding viewpoint selection

---

**Input:** Map  $\mathcal{M}$ , pUAV position  ${}^L\mathbf{x}_P$ , sUAV path  ${}^L\mathcal{P}_S$   
**Output:** Goal  ${}^L\mathbf{g}_P$  for the pUAV  
**Parameters:** raycasting sample count  $n_{\text{samples}}$ , raycasting max. ray length  $d_{\text{ray}}$ , min. safe distance  $d_{\text{buffer}}$  from the sUAV path, pUAV min. obstacle distance  $d_P$   
  ▷ Construct a safety buffer around the UAV path

- 1:  $\mathcal{B} \leftarrow \text{BUFFER}({}^L\mathcal{P}_S, d_{\text{buffer}})$    ▷ Single non-convex polygon
- 2:  $\mathcal{V}_{\text{all}} \leftarrow \emptyset$    ▷ Get a visibility region for each point in the path
- 3: **for**  $(\mathbf{p}_i, \theta_i) \in {}^L\mathcal{P}_S$  **do**
- 4:    $\mathcal{V} \leftarrow \emptyset$    ▷ Single non-convex polygon
- 5:   **for**  $\alpha \in \left(k \frac{2\pi}{n_{\text{samples}}}\right)_{k=0}^{n_{\text{samples}}}$  **do**
- 6:      $\mathbf{r}_{\text{end}} \leftarrow \mathbf{p}_i + [d_{\text{ray}} \cos \alpha, d_{\text{ray}} \sin \alpha, 0]^T$    ▷ get the first intersection with obstacle or  $\mathbf{r}_{\text{end}}$
- 7:      $\mathbf{r}_{\text{int}} \leftarrow \text{RAY\_OBSTACLE\_INTERSECT}(\mathcal{M}, \mathbf{p}_i, \mathbf{r}_{\text{end}})$
- 8:      $\mathcal{V}.add(\mathbf{r}_{\text{int}})$
- 9:    $\mathcal{V}_{\text{all}}.add(\mathcal{V} \setminus \mathcal{B})$
- 10:   ▷ Generate safe space region
- 11:    $\mathcal{S} \leftarrow \emptyset$    ▷ Multi-polygon
- 12:   **for**  $v \in \mathcal{M}[v_z = {}^Lx_{Pz}]$  **do**   ▷  $v$  is a single voxel
- 13:     **if**  $\text{OBS\_DIST}(v) > d_P$  and  $v \in \bigcup \mathcal{V}_{\text{all}}$  **then**
- 14:        $\mathcal{S} \leftarrow \mathcal{S} \cup \text{POLYGON}(v_x \pm \frac{r}{2}, v_y \pm \frac{r}{2})$    ▷ Do union with safe space region, adjacent polygons are joined
- 15:      $\mathcal{S}_{\text{closest}} \leftarrow \arg \min_{S_i \in \mathcal{S}} \text{DISTANCE}({}^L\mathbf{x}_P, S_i)$    ▷ Find intersection of safe region and the visibility regions
- 16:      $\mathcal{I}_{\text{all}} \leftarrow \mathcal{S}_{\text{closest}}$
- 17:      $i_{\text{found}} \leftarrow \text{false}$
- 18:     **for**  $\mathcal{V}_i \in \mathcal{V}_{\text{all}}$  **do**
- 19:        $\mathcal{I}_{\text{new}} \leftarrow \mathcal{I}_{\text{all}} \cap \mathcal{V}_i$    ▷ Intersection is a multi-polygon
- 20:       **if**  $\mathcal{I}_{\text{new}} = \emptyset$  **then**   ▷ No more intersections found
- 21:         **break**
- 22:       **else**
- 23:          $\mathcal{I}_{\text{all}} \leftarrow \mathcal{I}_{\text{new}}$
- 24:          $i_{\text{found}} \leftarrow \text{true}$
- 25:       **if**  $i_{\text{found}}$  **then**   ▷ Select goal as the closest pole of inaccessibility
- 26:          ${}^L\mathbf{g}_P \leftarrow \arg \min_{\text{POI}(\mathcal{I}_i), \mathcal{I}_i \in \mathcal{I}_{\text{all}}} \|\text{POI}(\mathcal{I}_i) - {}^L\mathbf{x}_P\|_2$
- 27:     **return**  ${}^L\mathbf{g}_P$

---

regions  $\mathcal{V}_{\text{all}}$  by performing raycasting from each waypoint  $\mathbf{p}_i$  to the surrounding voxels at the same altitude. The algorithm calculates the difference of the visibility regions and the safety buffer  $\mathcal{B}$ , finds the closest safe region  $\mathcal{S}_{\text{closest}}$  within  $\bigcup \mathcal{V}_{\text{all}}$ , and finds the intersection of  $\mathcal{S}_{\text{closest}}$  with as many visibility regions  $\mathcal{V}_i$  as possible. If such an intersection exists, the viewpoint  ${}^L\mathbf{g}_P$  is selected as the interior point that is furthest from the boundaries, i.e., the pole of inaccessibility (function  $\text{POI}()$  in Alg. 2) of the obtained intersection. The polygonal operations were implemented using the *boost::geometry* C++ library<sup>2</sup>.

2) *Guiding:* The *Multi-UAV path planner* transforms the sUAV path  ${}^L\mathcal{P}_S$  to the sUAV body frame  $S$  and removes all points  ${}^S\mathbf{p}_i \in {}^S\mathcal{P}_S$  such that  $\|{}^S\mathbf{p}_i\|_2 < \delta$ , where  $\delta$  is a distance threshold for considering the path waypoint as visited. The remaining path is transmitted to the sUAV over the wireless network and saved for the next guiding

<sup>2</sup><https://www.boost.org/libs/geometry/>

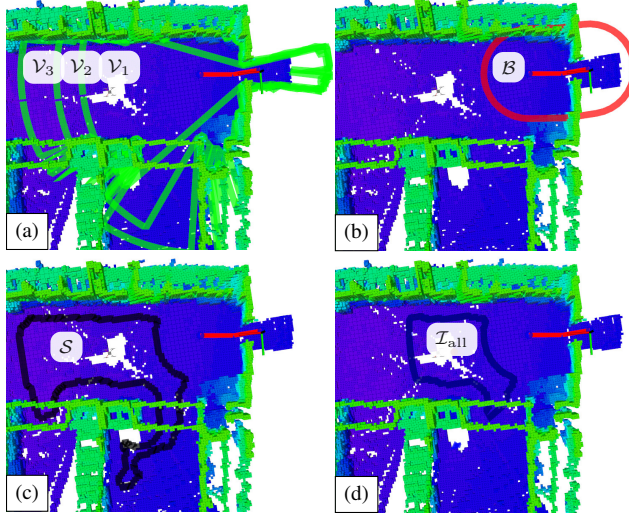


Fig. 4: Example of guiding viewpoint selection. sUAV path (red line) consists of 3 waypoints passing through the door in the upper right corner of the map. The algorithm constructs regions from which the waypoints are visible (a), a safety buffer around the sUAV path (b), safe space w.r.t. obstacles for the pUAV (c), and the final intersection  $\mathcal{I}_{\text{all}}$  (d).

step. It is worth mentioning that the planned path could instead be transmitted in the original frame  $L$  along with the transformation  ${}^V_L \mathbf{T}$  and transformed on board the sUAV. Transforming the path on board the pUAV minimizes the requirements imposed on the sUAV, making the approach compatible with a wide range of UAVs. The only requirements on the sUAV are the capability to transmit its local odometry in the local frame  $V$  and follow paths specified relatively to its current pose. The accuracy of the guiding process is subject to inaccuracies in the relative localization, drift of the UAV self-localization, and reliability of the communication between the UAVs.

### III. EXPERIMENTAL VERIFICATION

Two different quadrotor platforms (see Fig. 1) were utilized in the experimental evaluation. The pUAV was built upon the Holybro X500 frame, was  $0.7\text{ m} \times 0.7\text{ m}$  wide including propellers, and carried the Intel NUC 10i7FNH onboard computer with the Intel Core i7 10710U CPU, 16 GB of RAM, and a Wi-Fi module. The sUAV was built upon the DJI F330 frame, was  $0.45\text{ m} \times 0.45\text{ m}$  wide including propellers, and carried the Intel NUC 8i7BEH computer with the Intel Core i7-8559U CPU and 16 GB of RAM. Both UAVs used the Pixhawk 4 flight controller. The pUAV was equipped with the Ouster OSO-128 Rev C 3D LiDAR. The LiDAR has a  $360^\circ$  horizontal and  $90^\circ$  vertical Field Of View (FOV) and produces scans with a resolution of  $1024 \times 128$  beams at a rate of 10 Hz. Detailed information about the UAV hardware is available in [27], [28].

The pUAV utilized the LOAM algorithm [29] for self-localization. The sUAV carried a front-facing RealSense T265 tracking camera and utilized its stereo fisheye image and IMU output for VIO using the OpenVINS algorithm [30]. The sUAV was equipped with reflective markers

TABLE I: Parameters from the forest flight experiments.

Parameter	Symbol	Value
voxel size	$\mathcal{M}.\text{resolution}$	0.1 m
pUAV safe distance	$d_P$	0.9 m
sUAV safe distance	$d_S$	0.8 m
pUAV occ. space width	$w_P$	1.5 m
pUAV occ. space height	$h_P$	10 m
sUAV occ. space width	$w_S$	1.3 m
sUAV occ. space height	$h_S$	10 m
raycasting sample count	$n_{\text{samples}}$	500
raycasting max length	$d_{\text{ray}}$	6 m
min. safe distance from sUAV path	$d_{\text{buffer}}$	2 m

TABLE II: 2D straight-line distances traveled from the start of the guiding process by the sUAV in the forest. The distances were calculated from the LiDAR-based relative localization data.

Flight number	1	2	3	4	5
Distance traveled [m]	31.6	36.5	35.1	41.6	35.0

on its legs to aid the LiDAR-based relative localization. The software on board both UAVs was based on Ubuntu 20.04, Robot Operating System (ROS) 1, and the MRS UAV system [23]. Both UAVs were connected to a single Wi-Fi access point for mutual communication, and the Nimbrol network was used for transporting the ROS topics over the wireless network. The system time of the UAVs was synchronized using the chrony implementation of the NTP.

#### A. Cooperative flight through a forest

The pUAV was tasked to guide the sUAV through a forest (see Fig. 5 and the video attachment). The guiding process was triggered repeatedly, and the sUAV goal pose was generated by incrementing the sUAV pose by 4 m in the direction of the  $x$ -axis each time the guiding process finished (switched to the *GOAL REACHED* state). Table I contains parameters of the Algorithms 1 and 2 utilized in the forest flights.

Five separate flights were performed. Table II contains the distances traveled during these flights. The UAVs performed all of these flights successfully, flying until they reached a denser part of the forest, which was impossible to find a path through given the desired obstacle distance parameters. Fig. 6 shows the occupancy map built during one of the flights along with the trajectories traversed by the two UAVs.

The median processing time of the entire Alg. 1 was 8.9 s. The median processing times of the individual steps were 0.89 s for the guiding viewpoint selection (Alg. 2, Alg. 1 line 9), 0.60 s for pUAV path planning (Alg. 1 line 17), 5.33 s for sUAV path planning (Alg. 1 line 5), and the rest of the time was spent copying the occupancy maps and inserting occupied space into them. The processing time of pUAV path planning was much lower since the pUAV goal was always located in a safe space. In contrast, the sUAV goal was calculated by incrementing the sUAV pose and thus often laid too close to an obstacle, causing the planner to search for a path until a timeout threshold was reached.

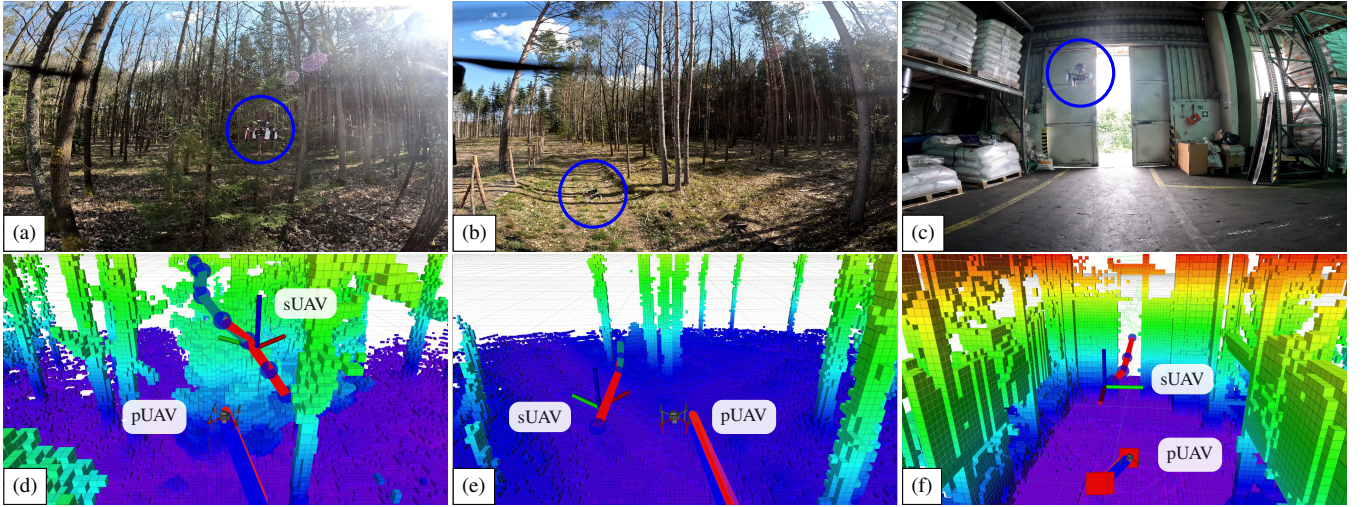


Fig. 5: Snapshots from the real-world experiments: images from the pUAV onboard camera (a-c) and visualization of the occupancy map and planned paths at the corresponding moments from similar viewpoints behind the pUAV (d-f). The sUAV is highlighted by blue circles.

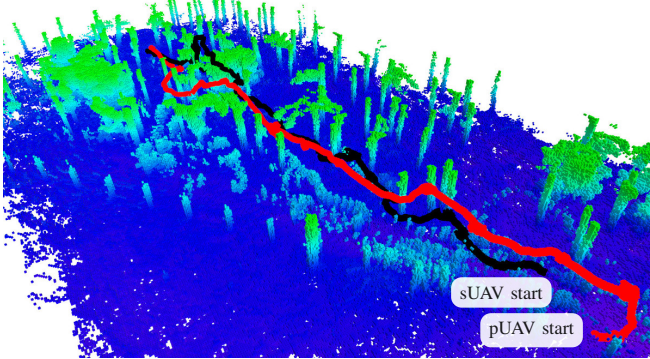


Fig. 6: Occupancy map from the flight through the forest along with the UAV trajectories (pUAV - red, sUAV - black). For clarity, the map visualization was sliced at the maximum height of 4 m above the ground.

### B. Guiding through a narrow gap

The pUAV was tasked to guide the sUAV through a narrow gap in an industrial warehouse environment (see Fig. 5 and the video attachment). The width of the gap and the safety distance of the path planner were gradually decreased to evaluate the performance of the proposed approach. The algorithms utilized the same parameters as in Table I, except for the sUAV safe distance  $d_S$ , which was decreased according to the width of the gap. Both UAVs started flying inside the warehouse, and the sUAV was guided through the narrow gap out of the building and back multiple times. Table III shows the results of this experiment. The evaluated guiding approach reached its limit when passing through a 0.9 m wide gap when the sUAV collided with the door during the fifth attempted pass due to an inaccuracy in the relative localization.

The achieved result corresponds to the expected performance given the used planner and relative localization method. Assuming that the width of the sUAV is 0.45 m between the tips of the propellers and the desired safety

TABLE III: Results of guiding the sUAV through narrow gaps with decreasing width. A single pass represents flight through the gap either out of the building or into the building.

Gap width [m]	1.2	1.1	1.0	0.9
sUAV safe distance $d_S$ [m]	0.5	0.45	0.4	0.4
Successful / attempted passes [-]	2/2	2/2	6/6	4/5

distance  $d_S$  of the planner between the center of the UAV and the closest occupied voxel is set to 0.4 m, the margin between the tips of the propellers and the occupied voxel is 0.175 m. In [22], the root mean squared error of the employed LiDAR-based relative localization method in the  $xy$ -plane during low-velocity maneuvers was quantified as 0.13 m. Using the A\* planner on the occupancy grid with voxels of size 0.1 m introduces an additional error due to discretization. Together, the possible errors reach the level of the safety margin, and collisions can occur.

## IV. CONCLUSIONS

A novel cooperative guiding framework enabling offloading the necessity to carry accurate but large and heavy obstacle-sensing sensors from a miniature UAV to another member of a UAV team while preserving the desired obstacle avoidance capabilities and reliable localization was proposed in this paper. To achieve such tight cooperation, the more-capable primary UAV performs occupancy mapping of the environment, relative localization of the less-capable secondary UAV, planning of collision-free paths for both the secondary UAV and itself, and guidance of the secondary UAV through the environment. The feasibility of the proposed approach was demonstrated in multiple real-world experiments in unknown cluttered GNSS-denied environments with all the algorithms running on board the UAVs with no external localization system nor external computational resources utilized.

## REFERENCES

[1] B. P. Duisterhof, S. Li, J. Burgués, V. J. Reddi, and G. C. H. E. de Croon, "Sniffy Bug: A Fully Autonomous Swarm of Gas-Seeking Nano Quadcopters in Cluttered Environments," in *IEEE/RSJ International Conference on Intelligent Robots and Systems (IROS)*, 2021, pp. 9099–9106.

[2] M. Petrik, P. Petracek, V. Kratky, T. Musil, Y. Stasinchuk, M. Vrba, T. Baca *et al.*, "UAVs Beneath the Surface: Cooperative Autonomy for Subterranean Search and Rescue in DARPA SubT," *Field Robotics*, vol. 3, pp. 1–68, 2023.

[3] D. Natter, K. Ening, and C. Paliotta, "An Incrementally Deployed Swarm of MAVs for Localization Using Ultra-Wideband," in *International Conference on Unmanned Aircraft Systems (ICUAS)*, 2022, pp. 497–505.

[4] I. Spasojevic, X. Liu, A. Ribeiro, G. J. Pappas, and V. Kumar, "Active Collaborative Localization in Heterogeneous Robot Teams," in *Proceedings of Robotics: Science and Systems*, Daegu, Republic of Korea, July 2023.

[5] L. Parker, B. Kannan, F. Tang, and M. Bailey, "Tightly-coupled navigation assistance in heterogeneous multi-robot teams," in *IEEE/RSJ International Conference on Intelligent Robots and Systems (IROS)*, vol. 1, 2004, pp. 1016–1022.

[6] J. Huang, S. Farritor, A. Qadi, and S. Goddard, "Localization and follow-the-leader control of a heterogeneous group of mobile robots," *IEEE/ASME Transactions on Mechatronics*, vol. 11, no. 2, pp. 205–215, 2006.

[7] A. Howard, L. E. Parker, and G. S. Sukhatme, "Experiments with a Large Heterogeneous Mobile Robot Team: Exploration, Mapping, Deployment and Detection," *The International Journal of Robotics Research*, vol. 25, no. 5-6, pp. 431–447, 2006.

[8] M. Hofmeister, M. Kronfeld, and A. Zell, "Cooperative visual mapping in a heterogeneous team of mobile robots," in *IEEE International Conference on Robotics and Automation*, 2011, pp. 1491–1496.

[9] M. A. Hsieh, A. Cowley, J. F. Keller, L. Chaimowicz, B. Grocholsky, V. Kumar, C. J. Taylor *et al.*, "Adaptive teams of autonomous aerial and ground robots for situational awareness," *Journal of Field Robotics*, vol. 24, no. 11-12, pp. 991–1014, 2007.

[10] P. Fankhauser, M. Bloesch, P. Krüsi, R. Diethelm, M. Wermelinger, T. Schneider, M. Dymczyk *et al.*, "Collaborative navigation for flying and walking robots," in *IEEE/RSJ International Conference on Intelligent Robots and Systems (IROS)*, 2016, pp. 2859–2866.

[11] S. Zhang, X. Zhang, T. Li, J. Yuan, and Y. Fang, "Fast Active Aerial Exploration for Traversable Path Finding of Ground Robots in Unknown Environments," *IEEE Transactions on Instrumentation and Measurement*, vol. 71, pp. 1–13, 2022.

[12] E. Mueggler, M. Faessler, F. Fontana, and D. Scaramuzza, "Aerial-guided navigation of a ground robot among movable obstacles," in *IEEE International Symposium on Safety, Security, and Rescue Robotics (2014)*, 2014, pp. 1–8.

[13] J. Delmerico, E. Mueggler, J. Nitsch, and D. Scaramuzza, "Active Autonomous Aerial Exploration for Ground Robot Path Planning," *IEEE Robotics and Automation Letters*, vol. 2, no. 2, pp. 664–671, 2017.

[14] A. Lakas, B. Belkhouché, O. Benkraouda, A. Shuaib, and H. J. Alasmawi, "A Framework for a Cooperative UAV-UGV System for Path Discovery and Planning," in *International Conference on Innovations in Information Technology (IIT)*, 2018, pp. 42–46.

[15] B. R. Chang, H.-F. Tsai, and J.-L. Lyu, "Drone-Aided Path Planning for Unmanned Ground Vehicle Rapid Traversing Obstacle Area," *Electronics*, vol. 11, no. 8, p. 1228, 2022.

[16] C. Chen, Y. Wan, B. Li, C. Wang, G. Xie, and H. Jiang, "Motion Planning for Heterogeneous Unmanned Systems under Partial Observation from UAV," in *IEEE/RSJ International Conference on Intelligent Robots and Systems (IROS)*, 2020, pp. 1474–1479.

[17] C. Shen, Y. Zhang, Z. Li, F. Gao, and S. Shen, "Collaborative air-ground target searching in complex environments," in *IEEE International Symposium on Safety, Security and Rescue Robotics (SSRR)*, 2017, pp. 230–237.

[18] J. Chen, Z. Chen, M. Fang, J. Li, Z. Ming, and S. Wang, "A GAN-based Active Terrain Mapping for Collaborative Air-Ground Robotic System," in *IEEE 4th International Conference on Advanced Robotics and Mechatronics (ICARM)*, 2019, pp. 622–627.

[19] T. Miki, P. Khrapchenkov, and K. Hori, "UAV/UGV Autonomous Cooperation: UAV assists UGV to climb a cliff by attaching a tether," in *International Conference on Robotics and Automation (ICRA)*, 2019, pp. 8041–8047.

[20] H. Masnavi, J. Shrestha, K. Kruusamäe, and A. K. Singh, "VACNA: Visibility-Aware Cooperative Navigation with Application in Inventory Management," *IEEE Robotics and Automation Letters*, 2023.

[21] V. Pritzl, M. Vrba, P. Stepan, and M. Saska, "Cooperative Navigation and Guidance of a Micro-Scale Aerial Vehicle by an Accompanying UAV using 3D LiDAR Relative Localization," in *International Conference on Unmanned Aircraft Systems (ICUAS)*. IEEE, 2022.

[22] V. Pritzl, M. Vrba, P. Štěpán, and M. Saska, "Fusion of Visual-Inertial Odometry with LiDAR Relative Localization for Cooperative Guidance of a Micro-Scale Aerial Vehicle," 2023, arXiv:2306.17544 [cs].

[23] T. Baca, M. Petrik, M. Vrba, V. Spurny, R. Penicka, D. Hert, and M. Saska, "The MRS UAV System: Pushing the Frontiers of Reproducible Research, Real-world Deployment, and Education with Autonomous Unmanned Aerial Vehicles," *Journal of Intelligent & Robotic Systems*, vol. 102, no. 1, p. 26, 2021.

[24] A. Hornung, K. M. Wurm, M. Bennewitz, C. Stachniss, and W. Burgard, "OctoMap: an efficient probabilistic 3D mapping framework based on octrees," *Autonomous Robots*, vol. 34, no. 3, pp. 189–206, 2013.

[25] M. Vrba, V. Walter, and M. Saska, "On Onboard LiDAR-based Flying Object Detection," 2023, arXiv:2303.05404 [cs].

[26] V. Krátký, P. Petráček, T. Báča, and M. Saska, "An autonomous unmanned aerial vehicle system for fast exploration of large complex indoor environments," *Journal of Field Robotics*, vol. 38, no. 8, pp. 1036–1058, 2021.

[27] D. Hert, T. Baca, P. Petracek, V. Kratky, V. Spurny, M. Petrik, V. Matous *et al.*, "MRS Modular UAV Hardware Platforms for Supporting Research in Real-World Outdoor and Indoor Environments," in *International Conference on Unmanned Aircraft Systems (ICUAS)*. IEEE, 2022.

[28] D. Hert, T. Baca, P. Petracek, V. Kratky, R. Penicka, V. Spurny, M. Petrik *et al.*, "MRS Drone: A Modular Platform for Real-World Deployment of Aerial Multi-Robot Systems," *Journal of Intelligent & Robotic Systems*, vol. 108, pp. 1–34, 2023.

[29] J. Zhang and S. Singh, "LOAM: Lidar Odometry and Mapping in Real-time," in *Robotics: Science and Systems*, 2014, pp. 109–111.

[30] P. Geneva, K. Eckenhoff, W. Lee, Y. Yang, and G. Huang, "OpenVINS: A Research Platform for Visual-Inertial Estimation," in *IEEE International Conference on Robotics and Automation (ICRA)*, 2020, pp. 4666–4672.